

## Supporting Information

# A metal–organic framework with suitable pore size and dual functionalities for highly efficient post-combustion CO<sub>2</sub> capture

Hui-Min Wen<sup>a</sup>, Caijun Liao<sup>a</sup>, Libo Li<sup>b,c</sup>, Ali Alsalme<sup>d</sup>, Zeid Alothman<sup>d</sup>, Rajamani Krishna<sup>e</sup>, Hui Wu<sup>f</sup>, Wei Zhou<sup>f\*</sup>, Jun Hu<sup>a\*</sup> and Banglin Chen<sup>b\*</sup>

<sup>a</sup> College of Chemical Engineering, Zhejiang University of Technology, Zhejiang, 310014, China. E-mail: hjzjut@zjut.edu.cn

<sup>b</sup> Department of Chemistry, University of Texas at San Antonio, One UTSA Circle, San Antonio, Texas 78249-0698, USA. Fax: (+1)-210-458-7428. E-mail: banglin.chen@utsa.edu

<sup>c</sup> College of Chemistry and Chemical Engineering, Taiyuan University of Technology, Taiyuan 030024, Shanxi, China

<sup>d</sup> Chemistry Department, College of Science, King Saud University, P O Box 2455, Riyadh 11451, Saudi Arabia

<sup>e</sup> Van't Hoff Institute for Molecular Sciences, University of Amsterdam, Science Park 904, 1098 XH Amsterdam, Netherlands

<sup>f</sup> NIST Center for Neutron Research, National Institute of Standards and Technology, Gaithersburg, MD 20899-6102, USA. E-mail: wzhou@nist.gov

**1. General Procedures and Materials.** All starting reagents and solvents were purchased from commercial companies and used without further purification. Powder X-ray diffraction (PXRD) patterns were performed by a Rigaku Ultima IV diffractometer operated at 40 kV and 44 mA with a scan rate of 2.0 deg min<sup>-1</sup>.

## 2. Fitting of pure component isotherms

The experimentally measured loadings for CO<sub>2</sub> measured at temperatures of 273 K, and 296 K in UTSA-120 and SIF-SIX-2-Cu-i were fitted with the dual-Langmuir-Freundlich isotherm model

$$q = q_{A,sat} \frac{b_A p^{v_A}}{1 + b_A p^{v_A}} + q_{B,sat} \frac{b_B p^{v_B}}{1 + b_B p^{v_B}} \quad (1)$$

with *T*-dependent parameters *b*<sub>A</sub>, and *b*<sub>B</sub>

$$b_A = b_{A0} \exp\left(\frac{E_A}{RT}\right); \quad b_B = b_{B0} \exp\left(\frac{E_B}{RT}\right) \quad (2)$$

The parameters are provided in Table S2.

The isotherm data for CH<sub>4</sub>, and N<sub>2</sub> measured at temperatures of 273 K, and 296 K in UTSA-120 and SIF-SIX-2-Cu-i were fitted with good accuracy with the single-site Langmuir model

$$q = q_{sat} \frac{bp}{1 + bp} \quad (3)$$

with *T*-dependent parameters

$$b = b_0 \exp\left(\frac{E}{RT}\right) \quad (4)$$

The parameters are provided in Table S3, and Table S4.

## 3. Virial Graph Analysis

Estimation of the isosteric heats of gas adsorption (*Q*<sub>st</sub>)

A virial-type expression of comprising the temperature-independent parameters *a*<sub>i</sub> and *b*<sub>j</sub> was employed to calculate the enthalpies of adsorption for CO<sub>2</sub> (at 273 K and 296 K) on UTSA-120a. In each case, the data were fitted use equation:

$$\ln P = \ln N + 1/T \sum_{i=0}^m a_i N_i + \sum_{j=0}^n b_j N_j \quad (5)$$

Here,  $P$  is the pressure expressed in Pa,  $N$  is the amount absorbed in mmol g<sup>-1</sup>,  $T$  is the temperature in K,  $a_i$  and  $b_j$  are virial coefficients, and  $m$ ,  $n$  represent the number of coefficients required to adequately describe the isotherms ( $m$  and  $n$  were gradually increased till the contribution of extra added  $a$  and  $b$  coefficients was deemed to be statistically insignificant towards the overall fit. And the average value of the squared deviations from the experimental values was minimized). The values of the virial coefficients  $a_0$  through  $a_m$  were then used to calculate the isosteric heat of absorption using the following expression:

$$Q_{st} = -R \sum_{i=0}^m a_i N_i \quad (6)$$

$Q_{st}$  is the coverage-dependent isosteric heat of adsorption and  $R$  is the universal gas constant. The heat enthalpy of CO<sub>2</sub> sorption for complex UTSA-120a in this manuscript are determined by using the sorption data measured in the pressure range from 0-1 bar (at 273 K and 296 K).

#### 4. IAST calculations

The adsorption selectivity is defined by

$$S_{ads} = \frac{q_1/q_2}{p_1/p_2} \quad (7)$$

In equation (7),  $q_1$ , and  $q_2$  are the molar loadings in the adsorbed phase in equilibrium with the bulk gas phase with partial pressures  $p_1$ , and  $p_2$ .

Figure 2d presents IAST calculations for binary 15/85 CO<sub>2</sub>/N<sub>2</sub> mixtures at 296 K. The CO<sub>2</sub> uptake is significantly higher in UTSA-120a as compared to SIF-SIX-2-Cu-i. The CO<sub>2</sub>/N<sub>2</sub> selectivity is about an order of magnitude higher in UTSA-120a as compared to SIF-SIX-2-Cu-i.

Figure S12 presents IAST calculations for 50/50 CO<sub>2</sub>/CH<sub>4</sub> mixtures at 296 K. Also in this case the separations are better in UTSA-120a as compared to SIF-SIX-2-Cu-i.

#### 5. Transient breakthrough of mixtures in fixed bed adsorbers

The performance of industrial fixed bed adsorbers is dictated by a combination of adsorption selectivity and uptake capacity. For a proper comparison of various MOFs, we perform transient

breakthrough simulations using the simulation methodology described in the literature.<sup>1,2</sup> For the breakthrough simulations, the following parameter values were used: length of packed bed,  $L = 0.3$  m; voidage of packed bed,  $\varepsilon = 0.4$ ; superficial gas velocity at inlet,  $u = 0.04$  m/s. The transient breakthrough simulation results are presented in terms of a *dimensionless* time,  $\tau$ , defined by dividing the actual time,  $t$ , by the characteristic time,  $\frac{L\varepsilon}{u}$ .

## Notation

$b_A$	Langmuir-Freundlich constant for species $i$ at adsorption site A, Pa $^{-\nu_{iA}}$
$b_B$	Langmuir-Freundlich constant for species $i$ at adsorption site B, Pa $^{-\nu_{iB}}$
$c_i$	molar concentration of species $i$ in gas mixture, mol m $^{-3}$
$c_{i0}$	molar concentration of species $i$ in gas mixture at inlet to adsorber, mol m $^{-3}$
$E$	energy parameter, J mol $^{-1}$
$L$	length of packed bed adsorber, m
$p_i$	partial pressure of species $i$ in mixture, Pa
$p_t$	total system pressure, Pa
$q_i$	component molar loading of species $i$ , mol kg $^{-1}$
$Q_{st}$	isosteric heat of adsorption, J mol $^{-1}$
$t$	time, s
$T$	absolute temperature, K
$u$	superficial gas velocity in packed bed, m s $^{-1}$

## Greek letters

$\varepsilon$	voidage of packed bed, dimensionless
$\nu$	Freundlich exponent, dimensionless
$\rho$	framework density, kg m $^{-3}$
$\tau$	time, dimensionless

## Subscripts

$i$	referring to component $i$
$t$	referring to total mixture

**Table S1.** The structural details for fully activated UTSA-120a, obtained from Rietveld refinement of the neutron diffraction data.

Unit cell parameters	UTSA-120a
Formula	C <sub>24</sub> H <sub>16</sub> CuF <sub>6</sub> N <sub>12</sub> Si
Formula weight	678.10
Crystal system	Tetragonal
Space group	I4/mmm
<i>a, b</i> (Å)	15.123(11)
<i>c</i> (Å)	7.8349(1)
$\alpha$ (°)	90.00
$\beta$ (°)	90.00
$\gamma$ (°)	90.00
<i>V</i> (Å <sup>3</sup> )	1791.89(34)
<i>Z</i>	2
<i>D</i> <sub>calcd</sub> (g cm <sup>-3</sup> )	1.257
<i>R</i> <sub>wp</sub> , <i>R</i> <sub>p</sub>	0.0207, 0.0170
CCDC	1882294

**Table S2.** Dual-Langmuir-Freundlich parameter fits for CO<sub>2</sub> in UTSA-120a and SIFSIX-2-Cu-i. The fits are based on experimental isotherm data at 296 K.

	Site A				Site B			
	$q_{A,\text{sat}}$ mol kg <sup>-1</sup>	$b_{A0}$ Pa <sup>-νA</sup>	$E_A$ kJ mol <sup>-1</sup>	$ν_A$ dimensionless	$q_{B,\text{sat}}$ mol kg <sup>-1</sup>	$b_{B0}$ Pa <sup>-νB</sup>	$E_B$ kJ mol <sup>-1</sup>	$ν_B$ dimensionless
UTSA-120a	0.57	4.81×10 <sup>-18</sup>	26.4	2.65	4.7	2.41×10 <sup>-11</sup>	31.3	1.34
SIF-SIX-2-Cu-i	2.4	7.87×10 <sup>-10</sup>	17.6	1.1	6	6.23×10 <sup>-12</sup>	34.8	1..14

**Table S3.** Langmuir parameter fits for CH<sub>4</sub> in UTSA-120a and SIFSIX-2-Cu-i. The fits are based on experimental isotherm data at 296 K.

	$q_{\text{sat}}$ mol kg <sup>-1</sup>	$b_0$ Pa <sup>-1</sup>	$E$ kJ mol <sup>-1</sup>
UTSA-120a	3.3	1.78×10 <sup>-8</sup>	13.3
SIF-SIX-2-Cu-i	5	9.89×10 <sup>-8</sup>	6.6

**Table S4.** Langmuir parameter fits for N<sub>2</sub> in UTSA-120a and SIFSIX-2-Cu-i. The fits are based on experimental isotherm data at 296 K.

	$q_{\text{sat}}$ mol kg <sup>-1</sup>	$b_0$ Pa <sup>-1</sup>	$E$ kJ mol <sup>-1</sup>
UTSA-120	1.75	$4.63 \times 10^{-9}$	14.6
SIF-SIX-2-Cu-i	4.1	$1.35 \times 10^{-7}$	4.3

**Table S5.** Comparison of the CO<sub>2</sub> adsorption capacity and CO<sub>2</sub>/N<sub>2</sub> selectivity of UTSA-120a with other high-performing materials at room temperature.

MOFs	Adsorption uptake		CO <sub>2</sub> /N <sub>2</sub> selectivity	$Q_{st}$ (kJ/mol)	Ref.
	0.15 bar (mmol g <sup>-1</sup> )	1.0 bar (mmol g <sup>-1</sup> )			
<b>UTSA-120a</b>	<b>3.56</b>	<b>5.0</b>	<b>600</b>	<b>27-31</b>	This work
Mg-MOF-74	5.31	8.04	148	47	3
Mg <sub>2</sub> (dobdc)(N <sub>2</sub> H <sub>4</sub> ) <sub>1.8</sub>	5.18	5.51	-	90	4
MAF-X25ox	4.08	7.1	250	43	5
Co-MOF-74	3.48	5.53	100	37	6
Zeolite 13X	3.47	-	30.4	37.2	6
Ni-MOF-74	3.21	5.80	30	42	6
Mg-dobpdc-mmen	3.14	4.0	262	70	7
SGU-29	2.65	3.53	3515	51.3	8
UTSA-16	2.64	4.3	314	34.6	6
SIFSIX-3-Ni	2.5	2.55	1874	52	9
SIFSIX-3-Cu	2.46	2.46	10500	54	10
SIFSIX-3-Zn	2.43	2.54	1800	45	11
CuBTTRi-mmen	2.38	4.17	166	96	12
NbOFFIVE-1-Ni	2.25	2.25	-	50	13
SIFSIX-2-Cu-i	2.11	5.41	140	31.9	11
Zn <sub>2</sub> (Atz) <sub>2</sub> (ox)	2.02	3.62	-	40.8	14
SERP-MOF-2	1.6	3.08	1084	33	15
SIFSIX-14-Cu-i	1.42	4.68	-	37.7	16
Bio-MOF-11	1.35	4.05	76.8	45	17
CPM-231	1.26	6.77	50	20.4	18
NJU-Bai8	1.2	2.51	58	37.7	19
Qc-5-Cu-sql	0.73	2.16	35000	36	20
PCN-88	0.69	4.20	18.1	27	21

**Table S6.** Comparison of the CO<sub>2</sub> adsorption capacity, CO<sub>2</sub>/CH<sub>4</sub> selectivity, and  $Q_{st}$  of UTSA-120a with other high-performing materials at room temperature.

MOFs	Adsorption uptake		CO <sub>2</sub> /CH <sub>4</sub> selectivity	$Q_{st}$ (kJ/mol)	Ref.
	0.15 bar (mmol g <sup>-1</sup> )	1.0 bar (mmol g <sup>-1</sup> )			
<b>UTSA-120a</b>	<b>3.56</b>	<b>5.0</b>	<b>96</b>	<b>27-31</b>	This work
Qc-5-Cu-sql	0.73	2.16	3300	36	20
SIFSIX-3-Zn	2.43	2.54	231	45	11
Mg-MOF-74	5.31	8.04	105	47	6
NaX	-	4.81	60	34.5	6
SIFSIX-2-Cu-i	2.11	5.41	33	31.9	11
UTSA-16	2.64	4.3	29.8	34.6	6
NJU-Bai8	1.2	2.51	15.9	37.7	19
Cu-TDPAT	1.73	5.09	13.8	42.2	22
ZIF-78	1.04	2.05	10.6	29	6
HKUST-1	1.15	5.44	7.4	35	6
Zn-MOF-74	1.83	5.32	5.0	31.7	23

**Table S7.** The structural details of the CO<sub>2</sub>-loaded sample (UTSA-120a·2.6CO<sub>2</sub>), obtained from Rietveld refinement of the neutron diffraction data.

Unit cell parameters of UTSA-200·2.6CO <sub>2</sub>	
Formula	C <sub>26.60</sub> H <sub>16.00</sub> CuF <sub>6</sub> N <sub>12.00</sub> O <sub>5.20</sub> Si
Formula weight	792.47
Temperature/K	300
Crystal system	Tetragonal
Space group	I4/mmm
<i>a</i> (Å)	15.1068(7)
<i>b</i> (Å)	15.1068(7)
<i>c</i> (Å)	7.9980(8)
$\alpha$ (°)	90.0
$\beta$ (°)	90.0
$\gamma$ (°)	90.0
<i>V</i> (Å <sup>3</sup> )	1825.3(4)
<i>Z</i>	2
<i>R</i> <sub>wp</sub> , <i>R</i> <sub>p</sub>	0.0238, 0.0198
CCDC number	1881280

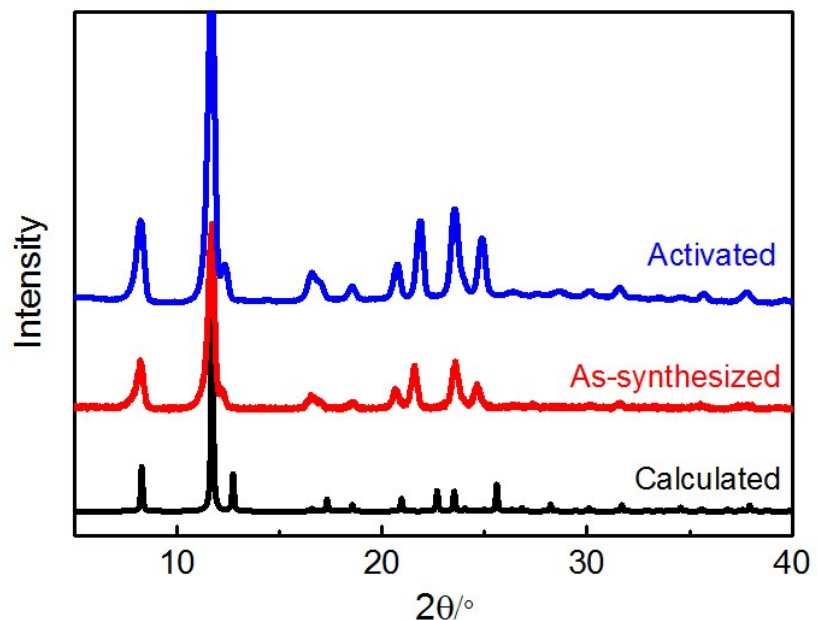


**Figure S1.** PXRD patterns of as-synthesized UTSA-120 (red) and activated UTSA-120a (blue) along with the calculated XRD pattern based on the neutron diffraction structure of UTSA-120a (black).

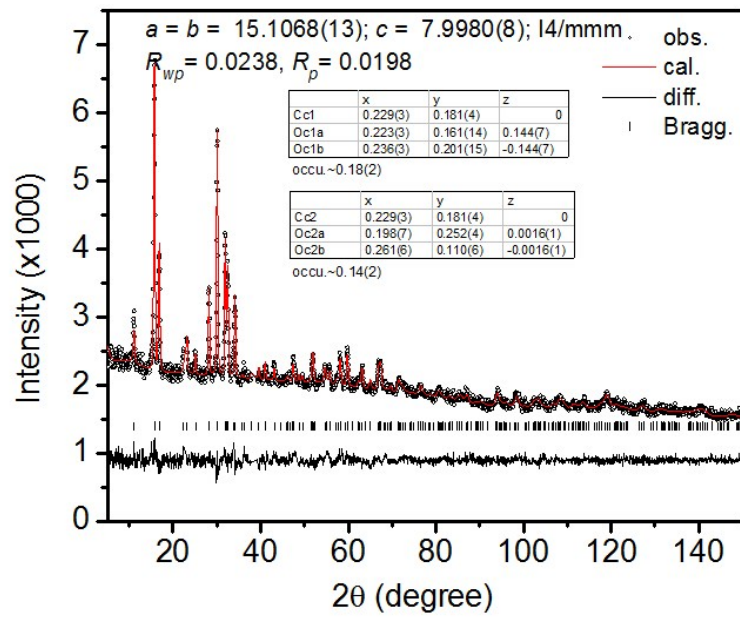
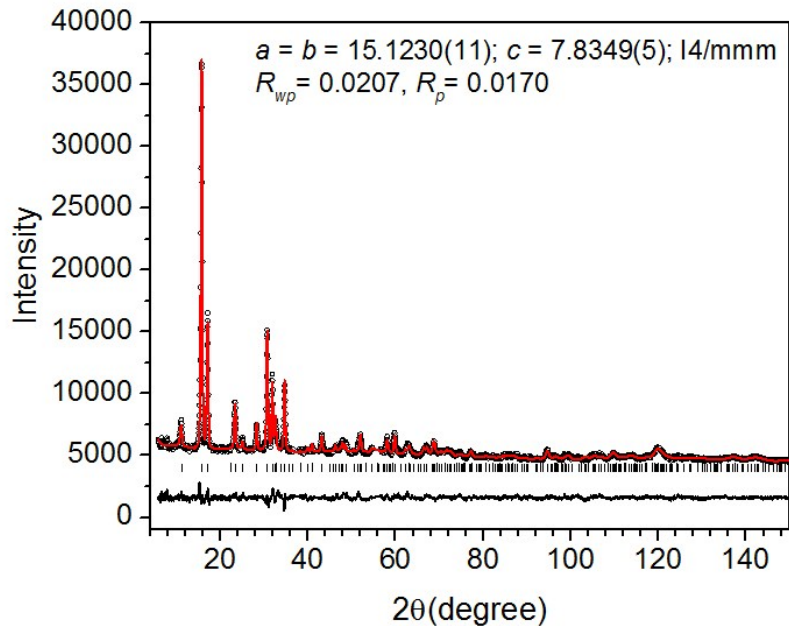


**Figure S2.** Rietveld refinements of the neutron powder diffraction data for bare UTSA-120a (the upper panel) and CO<sub>2</sub>-loaded UTSA-120a (the lower panel). The goodness of fit data and the refined CO<sub>2</sub> locations are shown in inset.

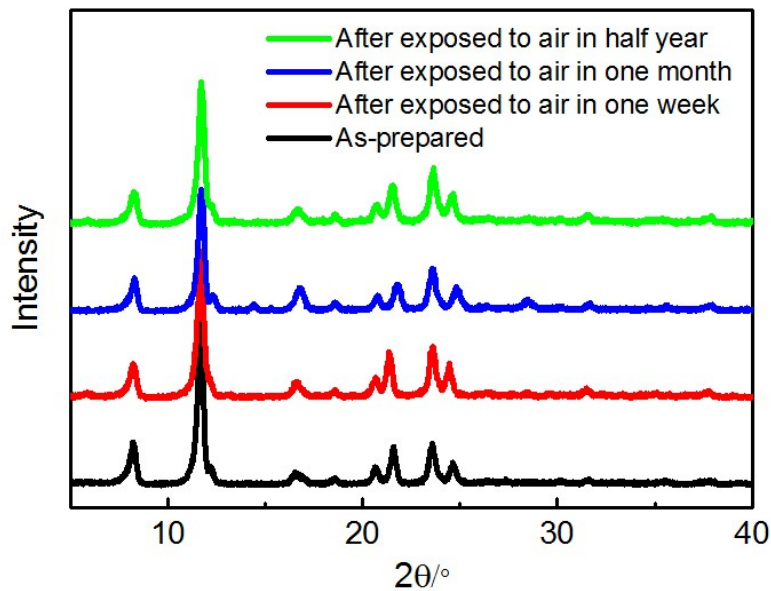


**Figure S3.** Experimental PXRD patterns of as-synthesized UTSA-120 sample and the sample after exposure to the air for one week, one month and half year, respectively, indicating its good stability toward moisture.

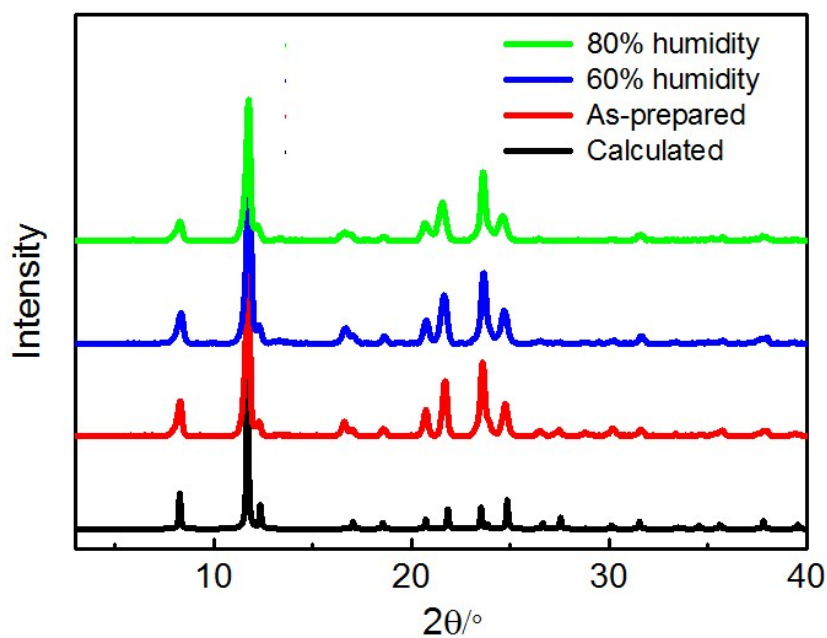


**Figure S4.** Experimental PXRD patterns of as-synthesized UTSA-120 sample and the sample exposed to variable humidity levels for one day.

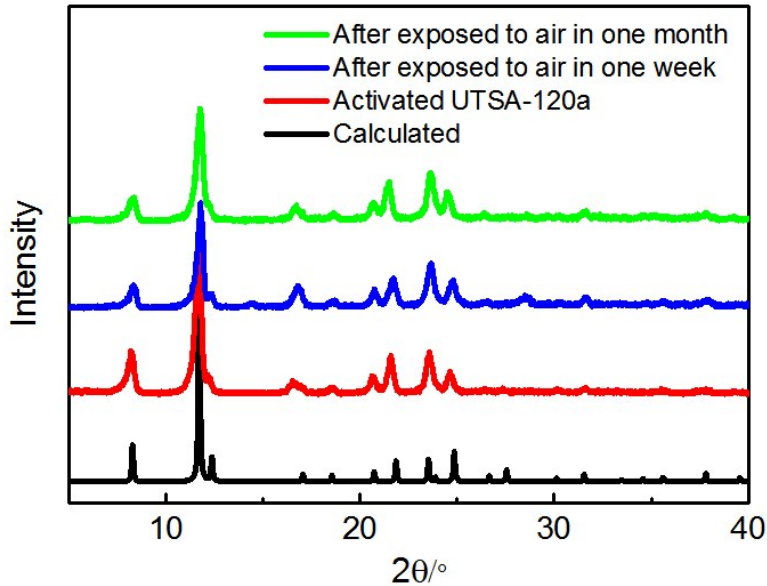


**Figure S5.** Experimental PXRD patterns of the activated UTSA-120a sample and the sample after exposure to air for one week and one month, respectively, indicating that the framework of UTSA-120a can be retained.

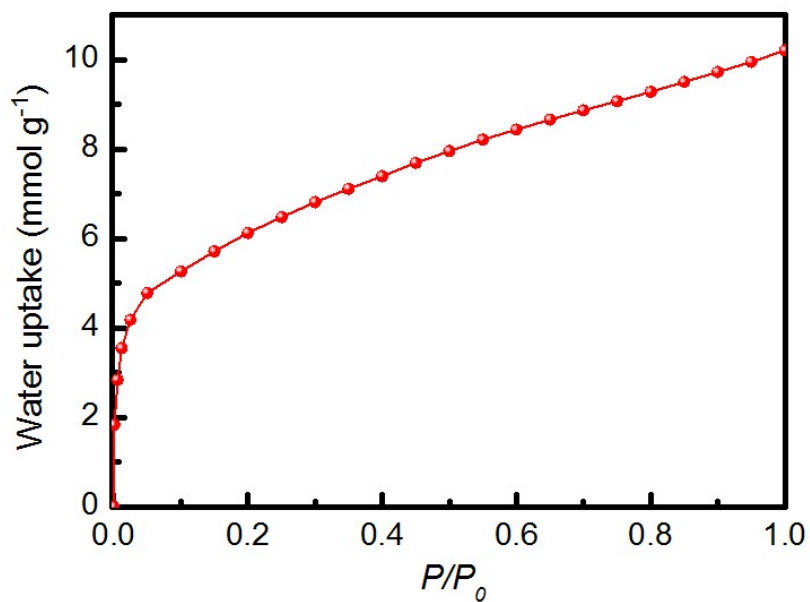


**Figure S6.** Water vapor sorption isotherms of UTSA-120a at room temperature.

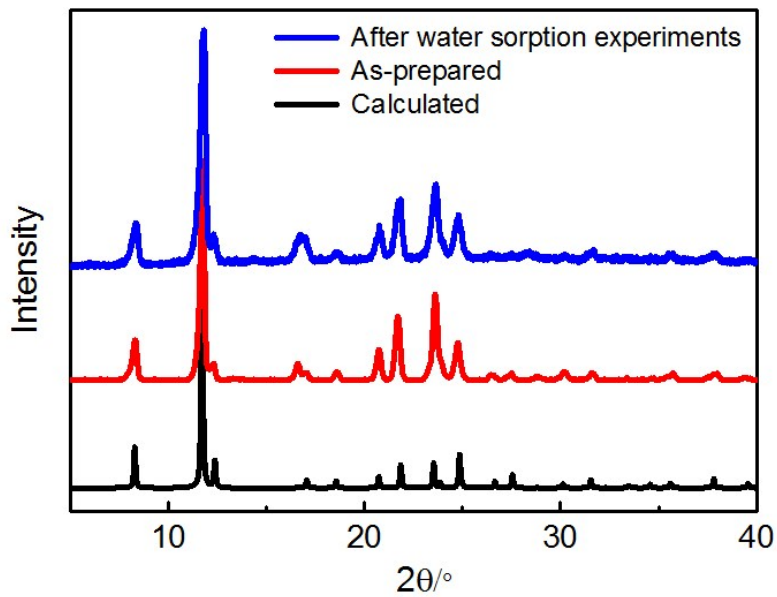


**Figure S7.** PXRD patterns of the UTSA-120a sample after water vapor sorption experiments, compared with the as-synthesized sample.

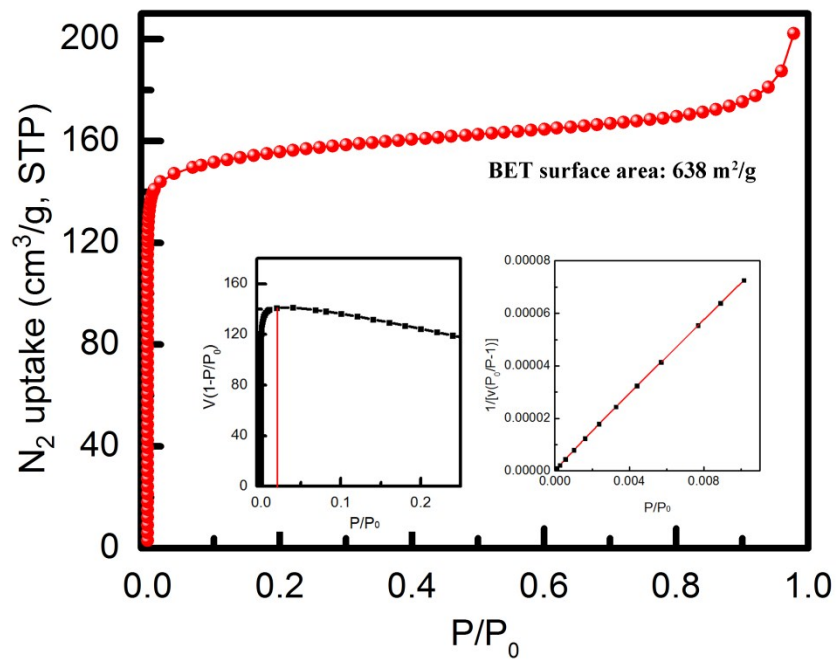


**Figure S8.** Nitrogen isotherm at 77 K with consistency and BET plots for the activated UTSA-120a sample.

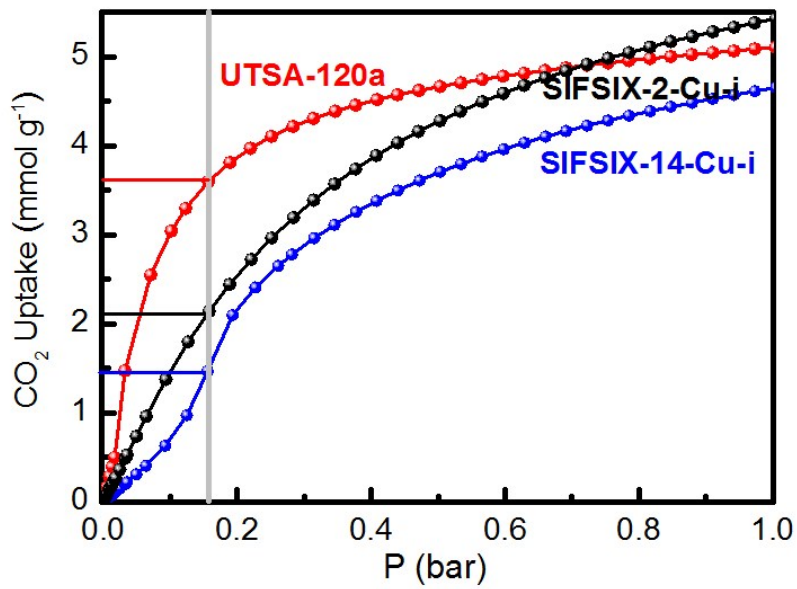


**Figure S9.** Comparison of  $\text{CO}_2$  sorption isotherms and capture capacity (at 0.15 bar and room temperature) for UTSA-120a with SIFSIX-2-Cu-i and SIFSIX-14-Cu-i.

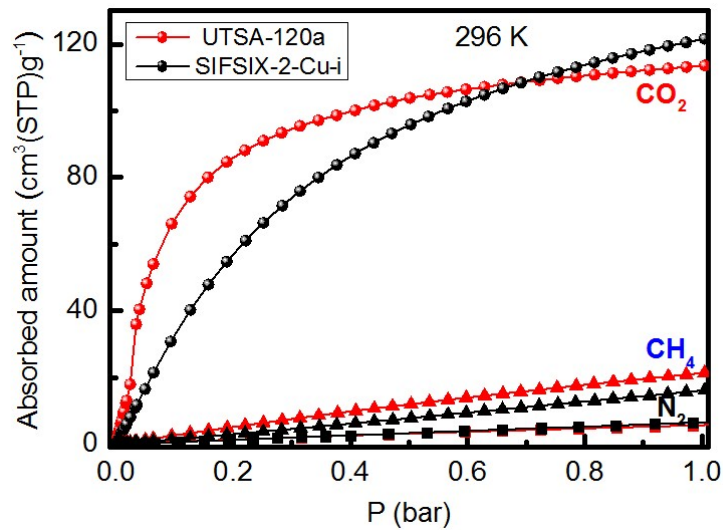


**Figure S10.** Adsorption isotherms of  $\text{CO}_2$  (circles),  $\text{CH}_4$  (triangles) and  $\text{N}_2$  (squares) for UTSA-120a (red) and SIFSIX-2-Cu-i (black) at 296 K up to 1 bar.

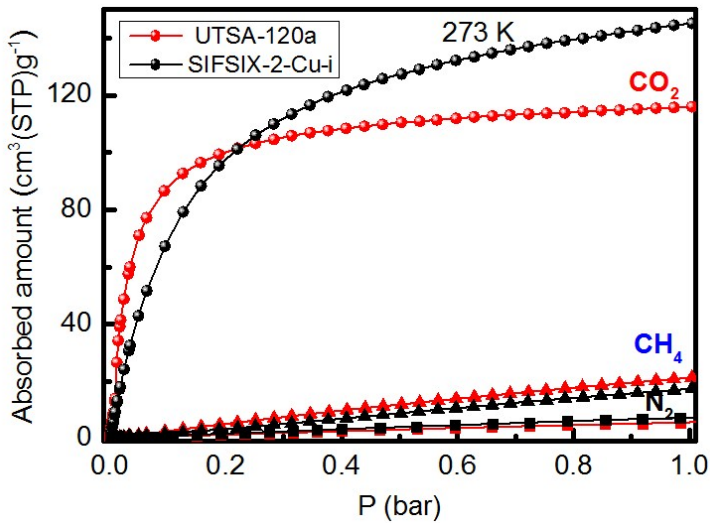


**Figure S11.** Adsorption isotherms of  $\text{CO}_2$  (circle),  $\text{CH}_4$  (triangle) and  $\text{N}_2$  (square) for UTSA-120a (red) and SIFSIX-2-Cu-i (black) at 273 K up to 1 bar.

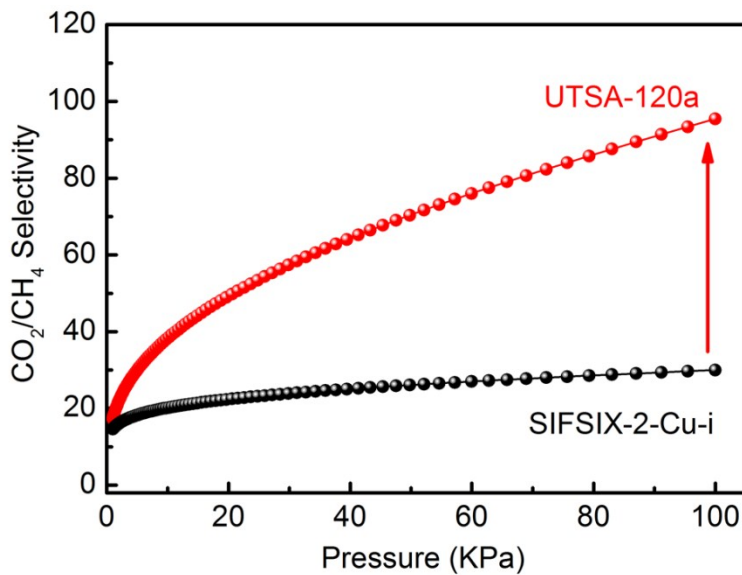


**Figure S12.** IAST selectivity of UTSA-120a (red) for  $\text{CO}_2/\text{CH}_4$  (50/50, v/v) at 296 K, as compared with SIFSIX-2-Cu-i (black).

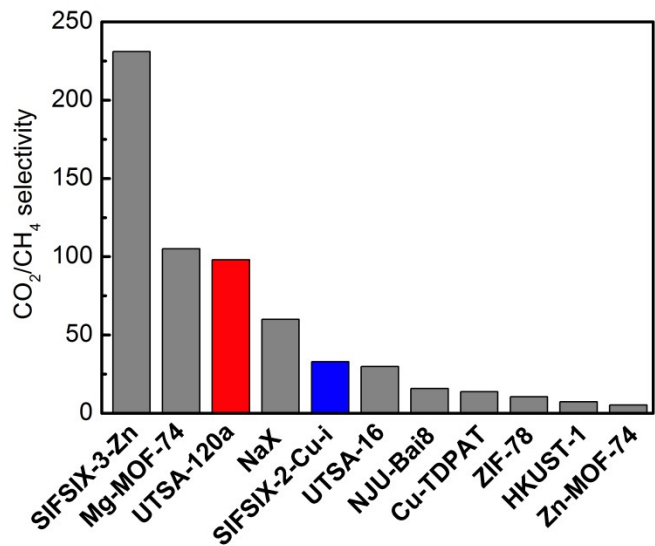


**Figure S13.** Comparison of IAST selectivity of UTSA-120a versus the other best-performing materials for  $\text{CO}_2/\text{CH}_4$  (50/50) separation.

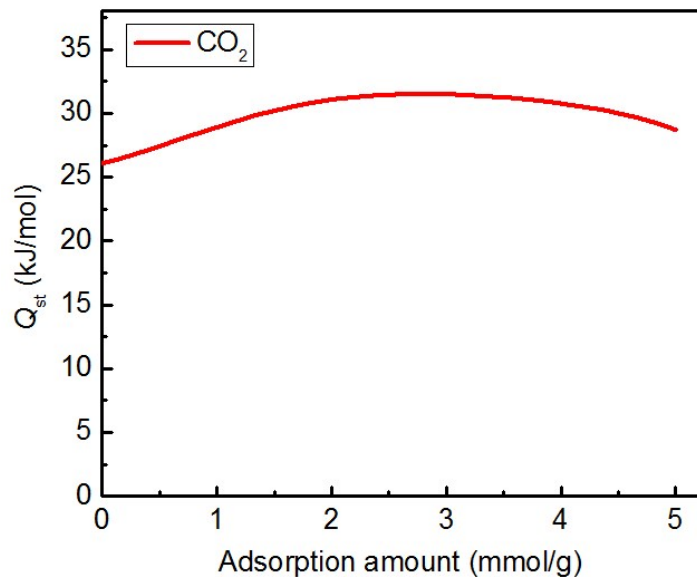


**Figure S14.** Heats of adsorption ( $Q_{\text{st}}$ ) of  $\text{CO}_2$  for UTSA-120a.

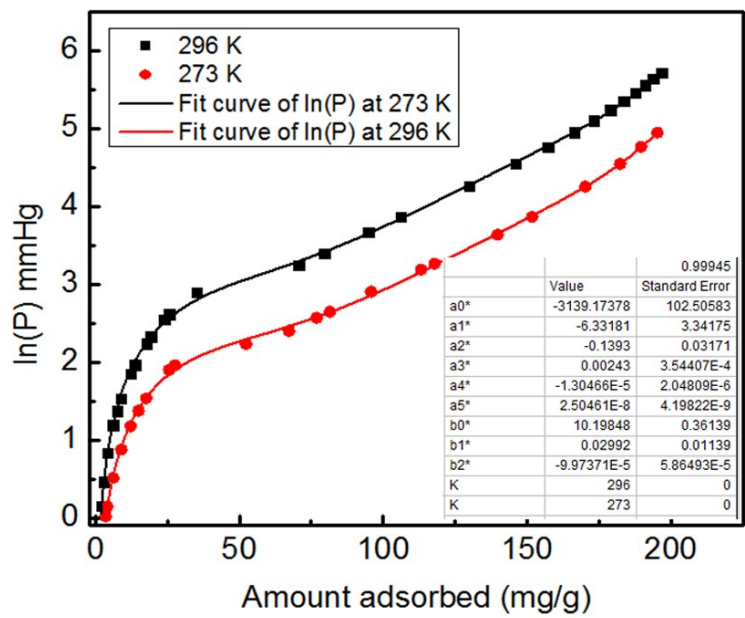


**Figure S15.** Virial fitting of the  $\text{CO}_2$  adsorption isotherms for UTSA-120a.

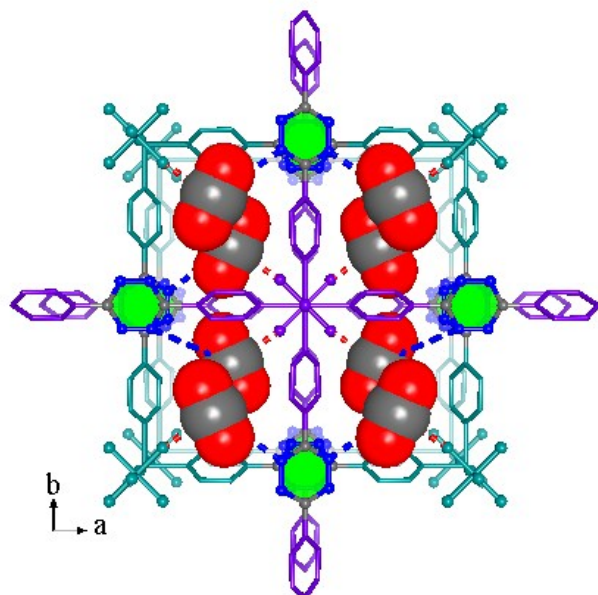


**Figure S16.** The binding sites and packing of  $\text{CO}_2$  molecules in the channels of UTSA-120a, viewed along the  $c$  axis.

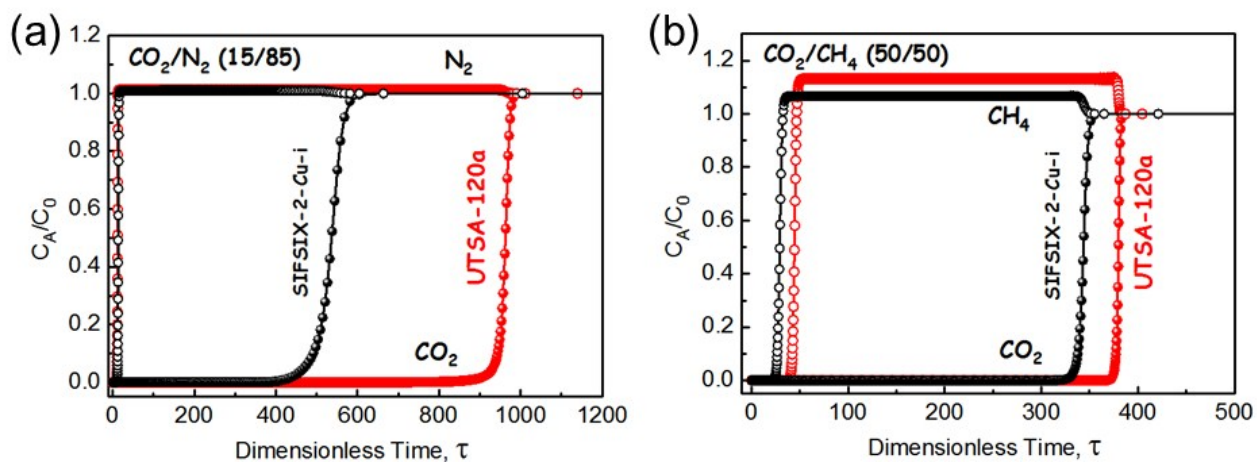


**Figure S17.** Transient breakthrough simulations of (a)  $\text{CO}_2/\text{N}_2$  (15:85, v/v) mixture (b)  $\text{CO}_2/\text{CH}_4$  (50:50) mixture on UTSA-120a versus SIFSIX-2-Cu-i at 298 K.

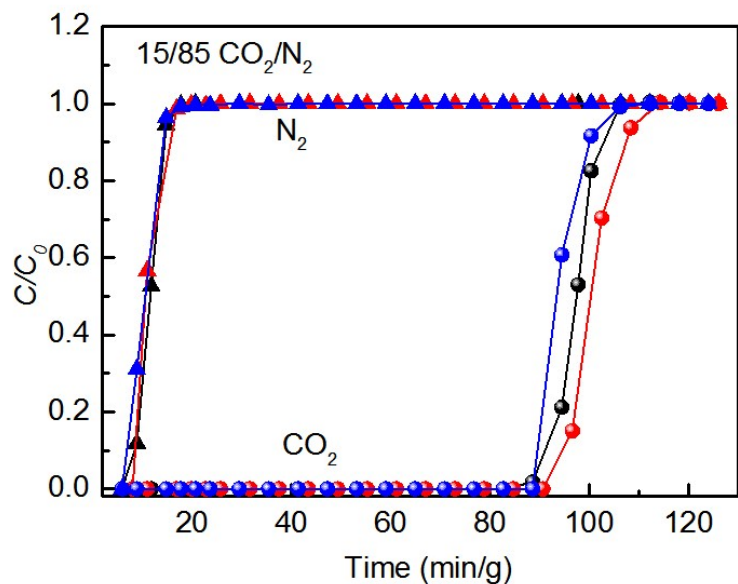


**Figure S18.** Cycling column breakthrough curves for  $\text{CO}_2/\text{N}_2$  separation (15/85, v/v) with UTSA-120a at 298 K and 1.01 bar. The breakthrough experiments were carried out in a column packed with UTSA-120a ( $\Phi 4.0 \times 150$  mm) at a flow rate of 2 mL/min.

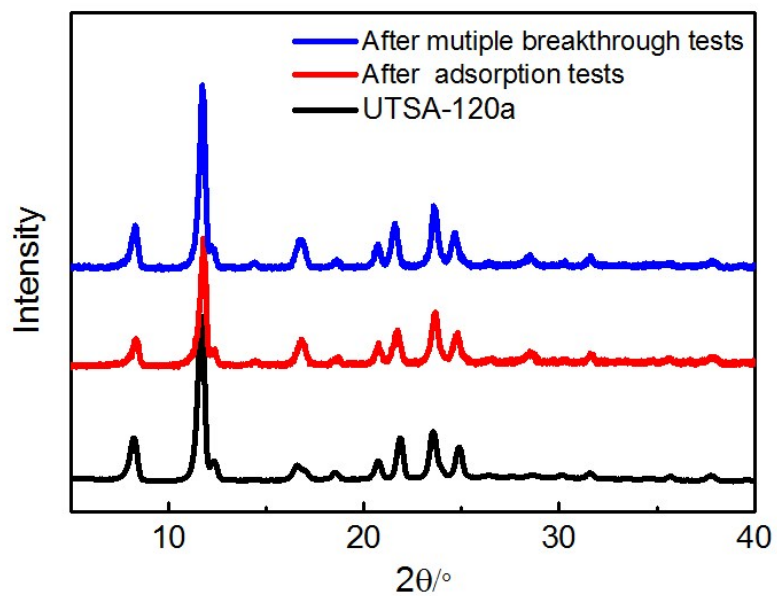


**Figure S19.** PXRD patterns of as-synthesized samples (black) and the samples after the adsorption tests (red) and multiple breakthrough tests (blue).

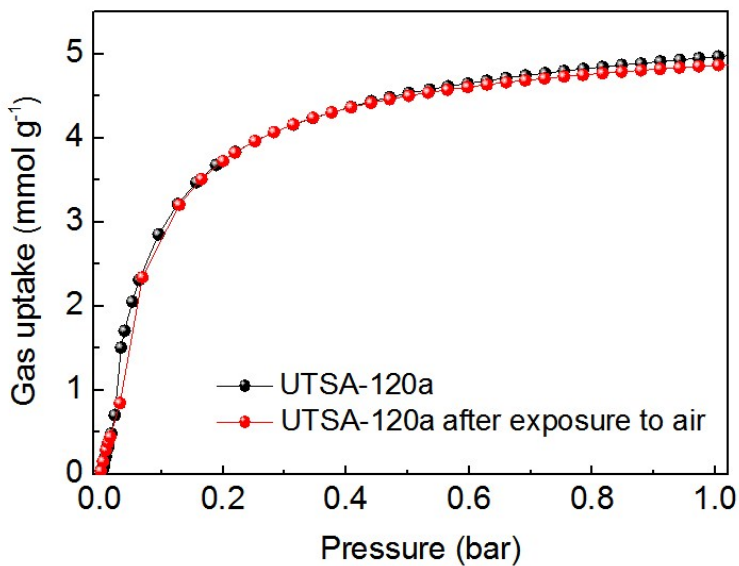


**Figure S20.** Comparison of CO<sub>2</sub> adsorption isotherms of UTSA-120a (black) and the re-activated sample after the exposure to air (red) for one week, confirming its good chemical stability.

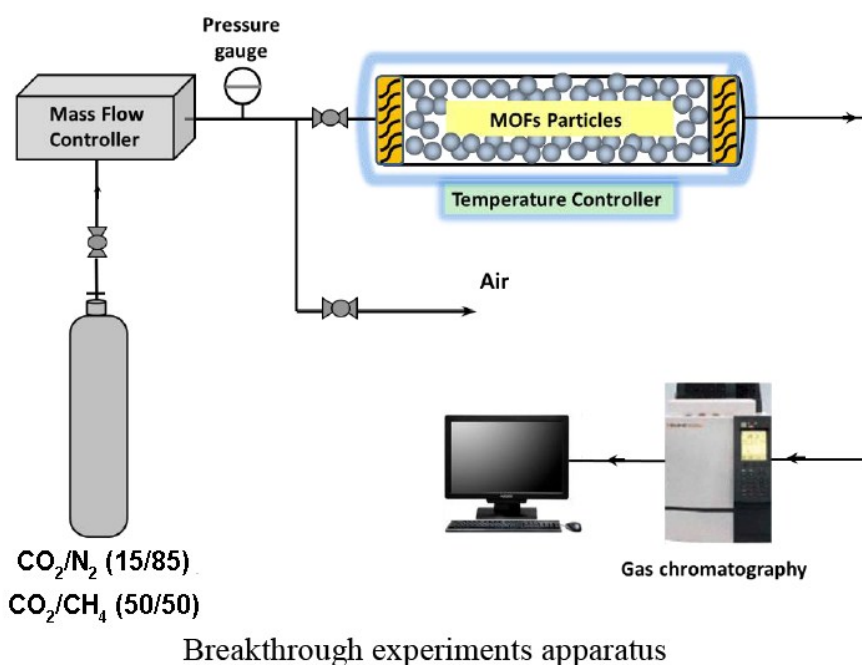


**Figure S21.** Schematic illustration of the apparatus for the breakthrough experiments.

## References

- [1] Krishna, R. The Maxwell-Stefan Description of Mixture Diffusion in Nanoporous Crystalline Materials. *Microporous Mesoporous Mater.* **2014**, *185*, 30–50.
- [2] Krishna, R. Methodologies for Evaluation of Metal-Organic Frameworks in Separation Applications. *RSC Adv.* **2015**, *5*, 52269–52295.
- [3] J. A. Mason, K. Sumida, Z. R. Herm, R. Krishna and J. R. Long, *Energy Environ. Sci.*, **2011**, *4*, 3030–3040.
- [4] P.-Q. Liao, X.-W. Chen, S.-Y. Liu, X.-Y. Li, Y.-T. Xu, M. Tang, Z. Rui, H. Ji, J.-P. Zhang and X.-M. Chen, *Chem. Sci.*, **2016**, *7*, 6528–6533.
- [5] P.-Q. Liao, H. Chen, D.-D. Zhou, S.-Y. Liu, C.-T. He, Z. Rui, H. Ji, J.-P. Zhang and X.-M. Chen, *Energy Environ. Sci.*, **2015**, *8*, 1011–1016.
- [6] S. Xiang, Y. He, Z. Zhang, H. Wu, W. Zhou, R. Krishna and B. Chen, *Nat. Commun.*, **2012**, *3*, 954.
- [7] T. M. McDonald, W. R. Lee, J. A. Mason, B. M. Wiers, C. S. Hong and J. R. Long, *J. Am. Chem. Soc.*, **2012**, *134*, 7056–7065.
- [8] S. J. Datta, C. Khumnoon, Z. H. Lee, W. K. Moon, S. Docao, T. H. Nguyen, I. C. Hwang, D. Moon, P. Oleynikov, O. Terasaki and K. B. Yoon, *Science*, **2015**, *350*, 302.
- [9] A. Kumar, D. G. Madden, M. Lusi, K.-J. Chen, E. A. Daniels, T. Curtin, J. J. Perry IV and M. J. Zaworotko, *Angew. Chem., Int. Ed.*, **2015**, *54*, 14372–14377.
- [10] O. Shekhah, Y. Belmabkhout, Z. Chen, V. Guillerm, A. Cairns, K. Adil and M. Eddaoudi, *Nat. Commun.*, **2014**, *5*, 4228.
- [11] P. Nugent, Y. Belmabkhout, S. D. Burd, A. J. Cairns, R. Luebke, K. Forrest, T. Pham, S. Ma, B. Space, L. Wojtas, M. Eddaoudi and M. J. Zaworotko, *Nature*, **2013**, *495*, 80–84.
- [12] A. Demessence, D. M. D’Alessandro, M. L. Foo and J. R. Long, *J. Am. Chem. Soc.*, **2009**, *131*, 8784.
- [13] P. M. Bhatt, Y. Belmabkhout, A. Cadiau, K. Adil, O. Shekhah, A. Shkurenko, L. J. Barbour and M. Eddaoudi, *J. Am. Chem. Soc.*, **2016**, *138*, 9301.
- [14] R. Vaidhyanathan, S. S. Iremonger, G. K. H. Shimizu, P. G. Boyd, S. Alavi and T. K. Woo, *Science*, **2010**, *330*, 650.

- [15] S. Nandi, S. Collins, D. Chakraborty, D. Banerjee, P. K. Thallapally, T. K. Woo and R. Vaidhyanathan, *J. Am. Chem. Soc.*, **2017**, *139*, 1734–1737.
- [16] M. Jiang, B. Li, X. Cui, Q. Yang, Z. Bao, Y. Yang, H. Wu, W. Zhou, B. Chen and H. Xing, *ACS Appl. Mater. Interfaces*, **2018**, *10*, 16628.
- [17] J. An, S. J. Geib and N. L. Rosi, *J. Am. Chem. Soc.* **2010**, *132*, 38–39.
- [18] Q.-G. Zhai, X. Bu, C. Mao, X. Zhao, L. Daemen, Y. Cheng, A. J. Ramirez-Cuesta and P. Feng, *Nat. Commun.*, **2016**, *7*, 13645.
- [19] L. Du, Z. Lu, K. Zheng, J. Wang, X. Zheng, Y. Pan, X. You and J. Bai, *J. Am. Chem. Soc.*, **2013**, *135*, 562–565.
- [20] K.-J. Chen, D. G. Madden, T. Pham, K. A. Forrest, A. Kumar, Q.-Y. Yang, W. Xue, B. Space, J. J. Perry IV, J.-P. Zhang, X.-M. Chen and M. J. Zaworotko, *Angew. Chem. Int. Ed.*, **2016**, *55*, 10268–10272.
- [21] J.-R. Li, J. Yu, W. Lu, L.-B. Sun, J. Sculley, P. B. Balbuena and H.-C. Zhou, *Nat. Commun.*, **2013**, *4*, 1538.
- [22] B. Li, Z. Zhang, Y. Li, K. Yao, Y. Zhu, Z. Deng, F. Yang, X. Zhou, G. Li, H. Wu, N. Nijem, Y. J. Chabal, Z. Lai, Y. Han, Z. Shi, S. Feng and J. Li, *Angew. Chem. Int. Ed.*, **2012**, *51*, 1412–1415.
- [23] F. Luo, C. Yan, L. Dang, R. Krishna, W. Zhou, H. Wu, X. Dong, Y. Han, T.-L. Hu, M. O’Keeffe, L. Wang, M. Luo, R.-B. Lin and B. Chen, *J. Am. Chem. Soc.*, **2016**, *138*, 5678–5684.